

1
2 **In situ electrical monitoring of SiO₂/Si structures in low-temperature**
3 **plasma using impedance spectroscopy**
4

5 Junki Morozumi*, Takahiro Goya, Tomohiro Kuyama,

6 Koji Eriguchi, and Keiichiro Urabe

7 *Department of Aeronautics and Astronautics, Graduate School of Engineering, Kyoto*
8 *University, Kyoto 615-8540, Japan*

9 * E-mail: morozumi.junki.74m@st.kyoto-u.ac.jp

10
11 **Abstract:**

12 To investigate the electrical properties and degradation features of dielectric materials
13 during plasma exposure, we developed an in situ impedance spectroscopy (IS) system.
14 We applied the proposed system to monitor SiO₂/Si structures exposed to Ar plasma. By
15 analyzing the measured data based on an equivalent circuit model considering the plasma
16 and SiO₂/Si structures, we obtained the resistance (*R*) and capacitance (*C*) values for the
17 SiO₂ film and SiO₂/Si interface. In a cyclic experiment of in situ IS and high-energy ion
18 irradiation, we characterized dielectric degradation by ion irradiation based on the
19 variations in the *R* and *C* values of the SiO₂ film. A continuous in situ IS measurement
20 revealed temporal variations in the electrical properties of the film and interface
21 independently. The thickness-dependent degradation observed for the *RC* variation was
22 analyzed and compared with the results of previous ex situ measurement studies. This
23 study demonstrates that the in situ IS measurement technique is promising for monitoring
24 plasma-assisted dry processes.

1. Introduction

In plasma-assisted dry processes such as plasma etching and plasma-enhanced chemical vapor deposition (PECVD), the properties of dielectric materials exposed to plasma are modified via physical and chemical interactions between the plasma and material surface.^{1,2)} In situ measurement methods for material surfaces have been developed to assess dielectric material modification during plasma exposure. For instance, in situ spectroscopic ellipsometry (SE) has been used to monitor the thickness of thin films during various dry processes.³⁻⁷⁾ In addition, in situ Fourier-transform infrared spectroscopy has been used to investigate surface reactions and chemical structures during PECVD processes.⁸⁻¹¹⁾ In addition to these structures and chemical properties, the electrical properties of dielectric films are critical targets for control in the design and fabrication of electronic devices.^{1,12)} Therefore, monitoring the electrical properties of dielectric films during plasma exposure is expected to be critical for further development of plasma-assisted dry processes.

The electrical properties of dielectric films modified through plasma exposure have been extensively investigated using ex situ measurement methods in terms of plasma process-induced damage.¹³⁻¹⁶⁾ Direct-current (DC)-based current–voltage (I – V) measurements have analyzed defect formation in dielectric films by comparing I – V curves before and after plasma exposure.¹⁷⁻¹⁹⁾ Alternating-current (AC)-based capacitance–voltage (C – V) measurements for metal–insulator–semiconductor structures have analyzed accumulated charges trapped in the defects and dielectric-constant variations.^{18,20-23)} In addition, AC-based conductance and admittance measurements have revealed frequency-dependent charge trapping and de-trapping features of the defects created near the dielectric–semiconductor interface via plasma exposure.²⁴⁻²⁶⁾ It is

1 expected that in situ measurements of these electrical properties during plasma processes
2 will contribute to the research and development of various plasma processes by providing
3 real-time and detailed time-dependent information on the electrical properties of
4 dielectric films.

5 To monitor the electrical properties of dielectric films deposited onto Si substrates
6 during plasma exposure, we employed an in situ impedance spectroscopy (IS) method.
7 The IS method measures the frequency dependence of complex impedance, which is the
8 impedance spectrum, and analyzes the electrical characteristics of target systems.²⁷⁻²⁹⁾
9 For the analysis of dielectric-film properties, the continuous operation of IS
10 measurements (time-dependent impedance spectroscopy [TDIS]) recently revealed
11 characteristic features of degradation and breakdown of dielectric thin films induced by
12 electric stresses.³⁰⁾ The IS measurement technique is widely used in research areas related
13 to electrochemical devices, and it can analyze multiphase (solid-liquid solution) systems,
14 such as Li-ion batteries and dye-synthesized solar cells.^{31,32)} Because the target system in
15 this study is a solid-plasma (charge-containing fluid) multiphase system, the IS
16 measurements have the potential of being an in situ monitoring method for the material
17 properties in plasmas. For example, in studies on the Langmuir probe method, resistive
18 surface-modified layers on metal probes formed by Hg and N₂ plasmas were detected
19 using the IS method.^{33,34)} Zanáška et al. measured semiconductor-film properties (Fe₂O₃
20 and TiO₂) during deposition processes measured using the in situ IS method.³⁵⁾ Based on
21 this background, we developed an in situ IS measurement system and an electrical circuit
22 model for analyzing the properties of dielectric films and dielectric-semiconductor
23 interface exposed to a low-temperature plasma.

24 In this paper, we report in situ IS measurements to reveal the electrical properties and

1 degradation features of SiO₂ films and SiO₂/Si interface placed in a surface-wave Ar
2 plasma. In the following sections, the principles and experimental procedures of the in
3 situ IS measurement method used in this study are explained. Next, the variation in the
4 electrical properties of the SiO₂ film and SiO₂/Si interface induced through high-energy
5 Ar ion (Ar⁺) irradiation is evaluated from impedance spectra obtained via a cyclic
6 experiment of in situ IS measurements and high-energy Ar⁺ irradiation. Based on the
7 results of continuous in situ IS measurements while maintaining the discharge conditions
8 (in situ TDIS), we characterized the temporal variation in the electrical properties of the
9 film and interface during plasma exposure. The features revealed by the in situ TDIS
10 measurements were compared with the results of ex situ optical and electrical
11 measurements before and after the plasma exposure.

12 13 **2. In situ impedance spectroscopy**

14 **2.1 Circuit model for SiO₂/Si structure in plasma**

15 Figure 1(a) shows a schematic of a low-pressure plasma chamber with a sample stage
16 at the bottom. When plasma is generated in the chamber, and a sample of the SiO₂/Si
17 structure is placed on the stage, the grounded chamber wall, ion sheath on the wall, plasma
18 bulk region, ion sheath on the SiO₂, SiO₂ film, SiO₂/Si interface, and Si substrate are
19 electrically connected in series. In this study, we investigated this series of systems using
20 the in situ IS method, focusing on the properties of the SiO₂ film and SiO₂/Si interface.

21 In an equivalent circuit model for the impedance spectra analysis, we ignored the
22 impedances of the plasma bulk region and the ion sheath on the chamber wall, considering
23 our plasma conditions and experimental setups. Because the plasma bulk region in this
24 study has an almost flat potential and the sheath on the chamber wall has a significantly

1 larger area than the sheath on the SiO₂ with an exposure area of approximately 300 mm²
2 (ϕ 20 mm), the resistances of these elements were negligible compared with other
3 elements.

4 When measurement frequencies are lower than the ion plasma frequency of the
5 generated plasma, the impedance of the ion sheath is expressed by the conventional
6 Langmuir probe theory.^{2,36)} In this study, an electric potential at the SiO₂ surface during
7 the measurements was maintained at a floating potential determined by the plasma
8 conditions, owing to the SiO₂ film and a capacitor blocking a DC current flow installed
9 in the measurement system. In this case, the sheath thickness is typically in the order of
10 micrometers, and it is significantly thicker than the nm-scale SiO₂ film and SiO₂/Si
11 interface. It requires higher measurement frequencies to analyze the capacitance
12 component of the ion sheath than to analyze the SiO₂ film and SiO₂/Si interface. Therefore,
13 the equivalent circuit for the sheath on the SiO₂ was modeled as a resistance R_{sh} in this
14 study (Fig. 1(b)).

15 The SiO₂ film and SiO₂/Si interface were modeled as parallels of resistance and
16 capacitance, as shown in Fig. 1(b). SiO₂ thin films are typically modeled as capacitances
17 in impedance analyses. However, because the resistivity of SiO₂ films in plasmas
18 significantly decreased from that under normal conditions owing to carrier generation via
19 vacuum-ultraviolet (VUV) photon irradiation from the plasma,³⁷⁻³⁹⁾ we adopted the
20 model in which the resistance, R_{ox} , is connected in parallel to the capacitance, C_{ox} , similar
21 to studies that measured sub-10-nm thin oxide films.^{30,40)} Another parallel RC circuit
22 model for the SiO₂/Si interface was based on the conductance method.^{24,25)} The resistance
23 R_{int} and capacitance C_{int} of the SiO₂/Si interface and their temporal variations during the
24 plasma exposure included features of defect formation near the interface.

1
2
3
4
5
6
7
8
9
10
11
12
13
14
15
16
17
18
19
20
21

2.2 Impedance-spectrum measurements with plasma

A fundamental circuit for the in situ IS measurements used in this study consisted of an AC voltage source, a sensing resistor R_s , and a blocking capacitor C_b (Fig. 2(a)). Unlike conventional impedance measurements using a commercially available impedance analyzer, the current sensing system was at the measurement-voltage application side and not on the ground side. This is because it is difficult to construct a current loop that comprises a plasma chamber. In addition, C_b is necessary for IS measurements with plasma because the electrical potential at the sample surface is determined by the floating potential. C_b maintains the potential structure of the system (electric field applied to the SiO_2 film and SiO_2/Si interface) and enables sensitive AC current sensing by blocking the DC current flow. The impedance of the target system, $\mathbf{Z}(\omega)$, was calculated from a complex voltage, $V_s(\omega) = X(\omega) + jY(\omega)$, which is a differential AC voltage between both ends of R_s , using Eq. (1) when the measurement frequency is $f = \omega/2\pi$.

$$\mathbf{Z}(\omega) = \frac{R_s}{X(\omega) + jY(\omega)} V_0 - R_s \quad (1)$$

Here, V_0 is the amplitude of the signal source voltage. By sweeping the angular frequency ω , the impedance at each frequency was obtained and plotted on the complex plane (Fig. 2(b)). It should be noted that capacitance C_b was ignored in the impedance calculations because its impedance, $1/j\omega C_b$, is significantly lower than those for the analyzed impedance values. In this study, based on the circuit model (Fig. 1(b)) considering the sheath, SiO_2 film, and SiO_2/Si interface, the impedance can be rewritten as follows.

$$\mathbf{Z}(\omega) = R_{\text{sh}} + \frac{R_{\text{int}}}{1 + j\omega R_{\text{int}} C_{\text{int}}} + \frac{R_{\text{ox}}}{1 + j\omega R_{\text{ox}} C_{\text{ox}}} \quad (2)$$

Each circuit parameter was obtained by fitting the measured impedance spectrum using

Eq. (2) based on the equivalent circuit model of the SiO₂/Si structure in the plasma.

3. Experimental

3.1 Setup

A schematic of the plasma chamber system employed in this study is shown in Fig. 3(a). The microwave was transferred to an antenna on a quartz window of the vacuum chamber. The input microwave power for plasma generation was 300 W. The chamber had an inner diameter of ~300 mm and a height of ~300 mm. High-purity Ar gas was fed into the chamber at a flow rate of 10 sccm. The gas pressure in the chamber was controlled at 10 Pa using a valve between the chamber and a turbomolecular pump. In this study, we generated surface-wave Ar plasma with an electron density, electron temperature, and floating potential of $1 \times 10^{11} \text{ cm}^{-3}$, 1.3 eV, and 23 V, respectively, measured by Langmuir probing. The Debye length for the plasma condition was 27 μm .²⁾ In the experimental step of high-energy Ar⁺ irradiation, we applied an AC bias voltage at 400 kHz to the sample stage through a matching box. In this step, the DC self-bias voltage and Ar⁺ flux to the sample were -1.0 kV and $6 \times 10^{14} \text{ cm}^{-2} \text{ s}^{-1}$, respectively.

A sample of the SiO₂/Si structure was set on the sample stage, electrically isolated from the chamber wall. The SiO₂ films measured in this study were deposited onto four-inch p-type Si substrates using a PECVD tool. The resistivity of the substrate was 0.1–0.5 $\Omega \text{ cm}$. The sample was compressed to the stage using a Teflon ring-shaped jig to maintain electric contact. The outer part of the sample surface was covered by a 4-mm-thick quartz ring, and the center hole of the ring with a diameter of 20 mm was the region of plasma exposure.

For the in situ IS measurements, we connected the measurement circuit shown in Fig.

1 3(b) to the sample stage. The 400 kHz biasing system was disconnected during the
2 measurements. When we performed the in situ IS measurements, the surface-wave plasma
3 on the sample was continuously generated, and it functioned as an electrode transmitting
4 the AC current. The measurement circuit elements were a function generator used for the
5 signal source. The sensing resistor $R_s = 1 \Omega$, and the blocking capacitor $C_b = 100 \mu\text{F}$.
6 $V_s(\omega)$ was measured using a lock-in amplifier operated in a differential-voltage-
7 measurement mode. We measured the impedance spectra at the frequency range of 30–
8 10^5 Hz with voltage amplitudes of 0.1–0.2 V_{pp} .

9 In addition to the in situ IS measurements, we obtained the optical and electrical
10 properties of SiO_2 films using ex situ measurement methods. The SE method was applied
11 to determine the variations in the optical thickness, refractive index, and extinction
12 coefficient before and after plasma exposure.^{17,19,41} I – V and C – V measurements were
13 performed using a Hg probe to investigate the variation in the leakage current and
14 dielectric constant.

16 3.2 Procedures

17 (1) Cyclic experiment of in situ IS measurements and high-energy ion irradiation

18 In this procedure (Fig. 4(a)), we investigated the effect of high-energy Ar^+ irradiation
19 on the SiO_2/Si structure. In the first step, we generated the surface-wave plasma and
20 measured the impedance spectrum of the SiO_2/Si structure. The system connected to the
21 sample stage in the first step was that for the in situ IS measurement (Fig. 3(b)). Then, we
22 replaced the system for the in situ IS measurement with that for the bias voltage
23 application (Fig. 3(a)), and irradiated high-energy Ar^+ ions to the substrate for 10 s. After
24 the high-energy Ar^+ irradiation, we replaced the system with that of the in situ IS

1 measurements again and recorded the impedance spectrum without the substrate biasing.
2 The high-energy Ar⁺ irradiation and in situ IS measurements were repeated for five cycles
3 in total. In addition to the above in situ IS measurements, the SiO₂-film thicknesses before
4 and after the experiment were measured using the ex situ SE method.

5 (2) *Continuous in situ IS measurements during plasma exposure (in situ TDIS)*

6 In this procedure (Fig. 4(b)), we attempted to evaluate the degradation features of the
7 SiO₂/Si structures during plasma exposure. We measured the impedance spectra of two
8 SiO₂/Si samples with SiO₂-film thicknesses of 97 and 20 nm. We repeatedly measured
9 the impedance spectra for 30 min with the duration of one frequency sweep at 1 min. The
10 discharge conditions were constant for 30 min; therefore, this measurement technique
11 monitored the temporal variation in the electrical properties of the SiO₂ film and SiO₂/Si
12 interface under the stress induced by plasma exposure with the same analogy to TDIS
13 originally developed to monitor the dielectric degradation under electric stress. By fitting
14 the measured impedance spectra, we obtained the resistance and capacitance values of
15 the SiO₂ film and SiO₂/Si interface at each measurement timing.

17 **4. Results and discussion**

18 **4.1 Modification of SiO₂ film via high-energy ion irradiation**

19 Figure 5 shows an impedance spectrum obtained in the first measurement step of
20 Procedure (1). Fig. 5(a) shows the total spectrum, and Fig. 5(b) is a focused view of the
21 spectrum in the low-impedance region. The influence of stray capacitances, such as
22 coaxial cables and the internal circuit of the lock-in amplifier, are eliminated in the
23 impedance spectra shown in Fig. 5 and the following. Two semicircles were observed in
24 the spectrum with a 1.3 kΩ offset in the real part. The offset (resistance at the high-

1 frequency edge of the spectrum) represents the sheath resistance R_{sh} , and the two
2 semicircles are RC elements, showing features of the SiO_2 film and SiO_2/Si interface,
3 respectively. The frequency range for the right-side (low-frequency) semicircle was 30
4 Hz –1 kHz , and that for the left-side (high-frequency) semicircle was 1–100 kHz .

5 Figure 6 shows the impedance spectra obtained after each step of high-energy Ar^+
6 irradiation. Fig. 6(a) shows the total spectra, and Fig. 6(b) shows a focused view of the
7 spectra in the low-impedance region. By high-energy Ar^+ irradiation for 50 s in total, the
8 optical thickness of the SiO_2 film decreased from 83 to 20 nm, as measured via ex situ
9 SE measurements. Because of the thickness decrease, the diameter of the RC component
10 for the SiO_2 film has to significantly decrease with increasing Ar^+ irradiation time.
11 Therefore, the right-side semicircle can be assigned the RC element of the SiO_2 film (R_{ox} ,
12 C_{ox}), and the left-side semicircle is regarded as the SiO_2/Si interface (R_{int} , C_{int}).

13 By fitting the spectra, we obtained the resistance and capacitance values of the SiO_2
14 film and SiO_2/Si interface as a function of the Ar^+ irradiation time, as shown in Fig. 7 ((a)
15 R_{ox} , (b) C_{ox} , (c) R_{int} , and (d) C_{int}). R_{ox} decreases linearly to the Ar^+ irradiation time, and
16 C_{ox} increases with a curve inversely proportional to the Ar^+ irradiation time. Compared
17 to the variations in R_{ox} and C_{ox} , the variation in R_{int} and C_{int} caused by the Ar^+ irradiation
18 is insignificant after 20 s. From the measured R_{ox} and C_{ox} values, we calculated the
19 variation in resistivity ρ_{ox} (Fig. 8(a)) and dielectric constant ϵ_{ox} (Fig. 8(b)) of the SiO_2
20 film, assuming that the decrease in thickness is linear to the Ar^+ irradiation time. The
21 decrease in ρ_{ox} is attributed to the influence of tunneling conduction by the decreased
22 thickness and/or defect formation acting as carrier hopping sites by high-energy Ar^+
23 irradiation. The gradual decrease in ϵ_{ox} suggests that microscopic SiO_2 structures
24 constructing local electric dipoles are modified by Ar^+ penetration into the film.

1 A comparison of the measured ρ_{ox} and ϵ_{ox} values obtained using the in situ IS method
2 with those using the ex situ measurements (I - V and C - V), for instance, those listed in
3 Table I, shows that the SiO₂ film in the plasma exhibits lower ρ_{ox} and higher ϵ_{ox} than that
4 under normal conditions. The significantly low ρ_{ox} measured under the plasma exposure
5 is attributed to the generation of electron-hole pairs via irradiation of VUV photons with
6 energies higher than the SiO₂ bandgap energy.³⁷⁻³⁹⁾ Under the experimental conditions in
7 this study, Ar atomic emission lines at 104 nm (11.8 eV) and 106 nm (11.6 eV) are the
8 main source of VUV photons.⁴²⁾ The increased ϵ_{ox} measured in the plasma is probably
9 owing to the decrease in the SiO₂-film thickness functioning as the dielectric. Because
10 the SiO₂ film conductivity near the surface is higher by the VUV irradiation, the film
11 considered as the dielectric is thinner than the SiO₂ film during the plasma exposure. This
12 results in the ϵ_{ox} values owing to the film thickness overestimation in the calculations.

13 The results show that the in situ IS measurements can assess the electrical properties
14 of the SiO₂ film modified by plasma exposure. After high-energy Ar⁺ irradiation, in
15 addition to the decrease in thickness, the impedance spectra indicated the variation in the
16 resistivity and dielectric constant of the SiO₂ film. These electrical features obtained using
17 in situ IS measurements are expected to facilitate the design and optimization processes
18 in electronic-device fabrication.

20 **4.2 Temporal change in SiO₂/Si properties monitored using in situ TDIS**

21 The electrical properties of the SiO₂/Si structures were continuously monitored via in
22 situ TDIS measurements (Procedure (2), Fig. 4(b)) to evaluate the modification of
23 dielectric properties during the plasma exposure under a condition without thickness
24 variation. In this experiment, we measured thick (97 nm) and thin (20 nm) SiO₂ samples

1 to investigate the effects of film thickness on the modification of electrical properties. We
2 also performed ex situ SE, $I-V$, and $C-V$ measurements before and after plasma exposure.
3 The ex situ measurement results are presented in Table I.

4 Figure 9 shows the impedance spectra obtained using in situ TDIS with the thick SiO₂
5 sample. For a high-impedance (low-frequency) part showing the SiO₂ film properties
6 (shown in Fig. 9(a)), a minimal change in the impedance spectra was observed. In another
7 part showing the SiO₂/Si interface properties (Fig. 9(b)), an increase in the semicircle
8 diameter was observed. This indicates that R_{int} increases during the plasma exposure. By
9 fitting the impedance spectra obtained every 1 min, we calculated the R and C values for
10 the SiO₂ film and SiO₂/Si interface as a function of plasma-exposure time (Fig. 10).
11 Unlike the high-energy Ar⁺ irradiation (Procedure (1), Fig. 4(a)), modification of the
12 resistivity and dielectric constant of the SiO₂ film (variations in R_{ox} (Fig. 10(a)) and C_{ox}
13 (Fig. 10(b)) were not observed. For the variation in SiO₂/Si interface properties, R_{int}
14 increased from ~15 min, reached the peak at 23 min, and then started to decrease (Fig.
15 10(c)). C_{int} monotonically increased from 10 to 14 nF during exposure (Fig. 10(d)).

16 The measurement results of the in situ TDIS using the thin SiO₂ sample are presented
17 in Figs. 11 (impedance spectra) and 12 (R and C values), respectively. Compared with the
18 results obtained for the thick SiO₂ sample, the gradual decrease in R_{ox} (Fig. 12(a)) and the
19 early turnover of R_{int} (Fig. 12(c)) were the significant differences. R_{int} turnover was the
20 decrease in the diameter of the left semicircle from 12 to 24 min in the impedance spectra
21 (Fig. 11). This suggests that in situ TDIS measurements can evaluate the thickness-
22 dependent degradation of dielectric films by plasma exposure. The optical thickness,
23 refractive index, and extinction coefficient of the SiO₂ film were slightly varied by the
24 plasma exposure, as confirmed from the ex situ SE results (Fig. 13).

1 The decrease in R_{ox} by the plasma exposure is attributed to the irradiation of VUV
2 photons with energies higher than the bandgap energy of the SiO_2 film, which breaks Si-
3 O bonds in the film.⁴³⁻⁴⁵⁾ Ishikawa et al. reported that the depth of E' centers (trivalent Si
4 centers in SiO_2) formed by the plasma exposure is ~ 10 nm,⁴⁵⁾ which is close to the
5 penetration depth value of VUV from Ar plasma.⁴⁴⁾ The difference in the degraded layer
6 ratio is the reason for the decrease in R_{ox} only in the thin SiO_2 sample. The decrease in
7 resistivity in the thin SiO_2 sample was also confirmed from the I - E curves and resistivity
8 values measured before and after the plasma exposure (Fig. 14 and Table I). The I - E
9 curves were plotted from the measured I - V curves, the flat-band voltages of the SiO_2/Si
10 structure obtained from the C - V measurements, and the film thicknesses measured by the
11 ex situ SE method.

12 The turnover observed for the resistance of the SiO_2/Si interface (R_{int} turnover) is
13 explained by the mechanisms shown in Fig. 15. In the earlier stage (Fig. 15(a)), VUV
14 photons penetrating the SiO_2 film formed electron-hole pairs in the film, and the holes
15 diffused and were trapped near the SiO_2/Si interface.⁴⁶⁻⁴⁸⁾ This increased the potential
16 barrier for the holes in the p-type Si substrate and caused R_{int} to increase. Negatively
17 charged (electron) trap sites were then formed in the SiO_2 film via continuous VUV
18 irradiation.⁴⁹⁾ The electron trap sites decreased the net positive charge near the interface
19 (Fig. 15(b)). The difference in the time constant of the hole and electron trap creation is
20 probably the reason for the R_{int} turnover. The thickness-dependent behavior of the R_{int}
21 turnover is attributed to the difference in the penetrated VUV photons and/or diffused
22 holes near the SiO_2/Si interface.

23 The increase in the capacitance of the SiO_2/Si interface (C_{int} increase) indicates an
24 increase in the total number of defects near the interface.⁵⁰⁾ Because the C values

1 measured using the IS method were a differential capacitance, the increase in C_{int}
2 indicated a number of charges that followed the measured AC voltage. The increase in
3 C_{int} observed for the thick SiO_2 sample suggests the contribution of VUV/UV photons
4 with lower energy values than the SiO_2 bandgap energy to the defects formed near the
5 SiO_2/Si interface. Shigetoshi et al.⁵¹⁾ observed that VUV/UV (> 130 nm) reaches the
6 SiO_2/Si interface and increases the interface trap density.

7 The in situ TDIS measurement results ensure that it can monitor the temporal variation
8 in electrical properties in the dielectric film and its back-side interface during plasma
9 exposure. The thickness-dependent property modification of the SiO_2/Si structures
10 exposed to the Ar plasma observed through the measurements must be considered in
11 further developments in nm-scale and atomic-scale plasma processes.

12 13 **5. Conclusion**

14 We developed an in situ measurement system for the electrical properties of dielectric
15 materials placed in plasmas. A new measurement system designed to perform the in situ
16 IS was tested to monitor the temporal variation in the electrical properties of SiO_2/Si
17 structures exposed to low-temperature Ar plasma. By analyzing the impedance spectra
18 obtained in a cyclic experiment of in situ IS measurements and high-energy Ar^+
19 irradiation, the impedance components of the SiO_2 film and SiO_2/Si interface were
20 assigned, and degradation of the SiO_2 film properties by high-energy Ar^+ irradiation was
21 detected. By continuous in situ IS measurements during the plasma exposure (in situ
22 TDIS), we determined the temporal variation in the electrical properties of the SiO_2 film
23 and SiO_2/Si interface independently. Thickness-dependent degradation features in the
24 resistivities of the SiO_2 film and SiO_2/Si interface were observed and analyzed, focusing

1 on the effect of VUV/UV photon irradiation on the film and interface. The experimental
2 results demonstrate that the proposed in situ IS measurement technique is promising for
3 monitoring dry processes utilizing plasma-material interaction.

4

1 **Acknowledgements**

2 This study was financially supported in part by Grant-in-Aid for Research Activity Start-
3 up (No. 18H05849) and Grant-in-Aid for Scientific Research (B) (No. 19H01886) from
4 the Japan Society for the Promotion of Science (JSPS), Japan. A part of this study was
5 supported by Kyoto University Nanotechnology Hub in “Advanced Research
6 Infrastructure for Materials and Nanotechnology Project” sponsored by the Ministry of
7 Education, Culture, Sports, Science and Technology (MEXT), Japan.

8

9

References

- 1) S. M. Sze, *VLSI Technology* (McGraw-Hill, New York, 1988) 2nd ed.
- 2) M. A. Lieberman and A. J. Lichtenberg, *Principles of Plasma Discharges and Materials Processing* (Wiley, Hoboken, 2005) 2nd ed.
- 3) I. P. Herman, *Optical Diagnostics for Thin Film Processing* (Academic Press, San Diego, 1996).
- 4) K. Tachibana, T. Shirafuji, Y. Hayashi, S. Maekawa and T. Morita, *Jpn. J. Appl. Phys.* **33**, 4191 (1994).
- 5) S. B. S. Heil, E. Langereis, A. Kemmeren, F. Roozeboom, M. C. M. van de Sanden and W. M. M. Kessels, *J. Vac. Sci. Technol. A* **23**, L5 (2005).
- 6) I. Volintiru, M. Creatore and M. C. M. van de Sanden, *J. Appl. Phys.* **103**, 033704 (2008).
- 7) D. Metzler, R. L. Bruce, S. Engelmann, E. A. Joseph and G. S. Oehrlein, *J. Vac. Sci. Technol. A* **32**, 020603 (2014).
- 8) Z. Zhou, E. S. Aydil, R. A. Gottscho, Y. J. Chabal and R. Reif, *J. Electrochem. Soc.* **140**, 3316 (1993).
- 9) S. M. Han and E. S. Aydil, *J. Vac. Sci. Technol. A* **14**, 2062 (1996).
- 10) S. Yokoyama, H. Goto, T. Miyamoto, N. Ikeda and K. Shibahara, *Appl. Surf. Sci.* **112**, 75 (1997).
- 11) T. Shirafuji, H. Motomura and K. Tachibana, *J. Phys. D: Appl. Phys.* **37**, R49 (2004).
- 12) S. M. Sze, *Semiconductor Devices: Physics and Technology* (Wiley, New York, 2008) 2nd ed.
- 13) K. Eriguchi and K. Ono, *J. Phys. D: Appl. Phys.* **41**, 024002 (2008).
- 14) K. Eriguchi, *J. Phys. D: Appl. Phys.* **50**, 333001 (2017).

- 1 15) K. Eriguchi, Jpn. J. Appl. Phys. **56**, 06HA01 (2017).
- 2 16) K. Eriguchi, Jpn. J. Appl. Phys. **60**, 040101 (2021).
- 3 17) Y. Nakakubo, A. Matsuda, M. Fukasawa, Y. Takao, T. Tatsumi, K. Eriguchi and K.
4 Ono, Jpn. J. Appl. Phys. **49**, 08JD02 (2010).
- 5 18) K. Shinohara, K. Nishida, K. Ono and K. Eriguchi, Jpn. J. Appl. Phys. **56**, 06HD03
6 (2017).
- 7 19) T. Kuyama and K. Eriguchi, Jpn. J. Appl. Phys. **57**, 06JD03 (2018).
- 8 20) M. Fukasawa, Y. Miyawaki, Y. Kondo, K. Takeda, H. Kondo, K. Ishikawa, M. Sekine,
9 H. Matsugai, T. Honda, M. Minami, F. Uesawa, M. Hori and T. Tatsumi, Jpn. J. Appl.
10 Phys. **51**, 026201 (2012).
- 11 21) M. Fukasawa, H. Matsugai, T. Honda, Y. Miyawaki, Y. Kondo, K. Takeda, H. Kondo,
12 K. Ishikawa, M. Sekine, K. Nagahata, F. Uesawa, M. Hori and T. Tatsumi, Jpn. J.
13 Appl. Phys. **52**, 05ED01 (2013).
- 14 22) K. Nishida, Y. Okada, Y. Takao, K. Eriguchi and K. Ono, Jpn. J. Appl. Phys. **55**,
15 06HB04 (2016).
- 16 23) T. Kamioka, Y. Hayashi, Y. Isogai, K. Nakamura and Y. Ohshita, AIP Adv. **7**, 095212
17 (2017).
- 18 24) E. H. Nicollian and A. Goetzberger, Bell Syst. Tech. J. **46**, 1055 (1967)
- 19 25) T. Kuyama, K. Urabe, M. Fukawsawa, T. Tatsumi and K. Eriguchi, Jpn. J. Appl. Phys.
20 **59**, SJJC02 (2020).
- 21 26) T. Kuyama, K. Urabe and K. Eriguchi, J. Appl. Phys. **131**, 133302 (2022).
- 22 27) J. R. Macdonald, Ann. Biomed. Eng. **20**, 289 (1992)
- 23 28) A. Lasia, *Electrochemical Impedance Spectroscopy and its Applications* (Springer,
24 New York, 2017).

- 1 29) E. Barsoukov and J. R. Macdonald, *Impedance Spectroscopy* (Wiley, Hoboken,
2 2018) 3rd ed.
- 3 30) T. Kuyama, K. Urabe and K. Eriguchi, Proc. 2021 IEEE International Reliability
4 Physics Symposium (IRPS), 2021, 4B.4.
- 5 31) A. Sacco, *Renew. Sustain. Energy Rev.* **79**, 814 (2017).
- 6 32) N. Meddings, M. Heinrich, F. Overney, J.-S. Lee, V. Ruiz, E. Napolitano, S. Seitz, G.
7 Hinds, R. Raccichini, M. Gaberšček and J. Park, *J. Power Sources* **480**, 228742
8 (2020).
- 9 33) R. A. Olson, *J. Appl. Phys.* **43**, 2785 (1972).
- 10 34) J. Morozumi, T. Kuyama, S. Kito, K. Urabe and K. Eriguchi, Ext. Abstr. (82nd
11 Autumn Meet., 2021); Japan Society of Applied Physics, 10a-S301-5a [in Japanese].
- 12 35) M. Zanaška, P. Kudrna, M. Čada, M. Tichý and Z. Hubička, *J. Appl. Phys.* **126**,
13 023301 (2019).
- 14 36) I. H. Hutchinson, *Principles of Plasma Diagnostics* (Cambridge University Press,
15 Cambridge, 2002) 2nd ed.
- 16 37) C. Cismaru and J. L. Shohet, *Appl. Phys. Lett.* **74**, 2599 (1999).
- 17 38) C. Cismaru and J. L. Shohet, *J. Appl. Phys.* **88**, 1742 (2000).
- 18 39) S. Samukawa, Y. Ishikawa, S. Kumagai and M. Okigawa, *Jpn. J. Appl. Phys.* **40**,
19 L1346 (2001).
- 20 40) M. Nath and A. Roy, *J. Mater. Sci.: Mater. Electron.* **26**, 3506 (2015).
- 21 41) A. Matsuda, Y. Nakakubo, Y. Takao, K. Eriguchi and K. Ono, *Thin Solid Films* **518**,
22 3481 (2010).
- 23 42) A. Kramida, Y. Ralchenko, J. Reader, and NIST ASD Team, NIST Atomic Spectra
24 Database (ver. 5.10), Available online, (2022).

- 1 43) K. Yokogawa, Y. Yajima, T. Mizutani, S. Nishimatsu and K. Suzuki, Jpn. J. Appl.
2 Phys. **29**, 2265 (1990).
- 3 44) T. Tatsumi, S. Fukuda and S. Kadomura, Jpn. J. Appl. Phys. **33**, 2175 (1994).
- 4 45) Y. Ishikawa, M. Okigawa, S. Samukawa and S. Yamasaki, J. Vac. Sci. Technol. B
5 **23**, 389 (2005).
- 6 46) M. H. Woods and R. Williams, J. Appl. Phys. **47**, 1082 (1976).
- 7 47) T. Yunogami, T. Mizutani, K. Suzuki and S. Nishimatsu, Jpn. J. Appl. Phys. **28**, 2172
8 (1989).
- 9 48) T. Yunogami, T. Mizutani, K. Tsujimoto and K. Suzuki, Jpn. J. Appl. Phys. **29**, 2269
10 (1990).
- 11 49) T. Kuyama, S. Yura, K. Urabe and K. Eriguchi, Proc. 42nd Int. Symp. Dry Process,
12 2021, p. 31.
- 13 50) S. Bottcher, N. Croitoru and A. Seidman, Proc. 18th Convention of Electrical and
14 Electronics Engineers in Israel, 1995, p. 5.5.3-1.
- 15 51) T. Shigetoshi, M. Fukasawa, K. Nagahata and T. Tatsumi, Jpn. J. Appl. Phys. **54**,
16 06GB05 (2015).
- 17

Figure captions

Figure 1: (Color online) (a) Schematic of SiO₂ film on Si substrate placed in plasma. (b) Serial circuit model for investigated structure considered in in situ IS measurements.

Figure 2: (Color online) (a) Fundamental configuration of in situ impedance spectroscopy (IS). (b) Complex impedance at angular frequency ω and impedance spectrum plotted by scanning ω in complex impedance plane.

Figure 3: (Color online) (a) Components for vacuum chamber, surface-wave plasma generation, and high-energy Ar⁺ irradiation used in experiments. (b) Electrical components and instruments for in situ IS measurements.

Figure 4: Diagrams of in situ IS measurement procedures. (a) Cyclic experiment with high-energy Ar⁺ irradiation. (b) Continuous measurement during plasma exposure (in situ TDIS).

Figure 5: Example impedance spectrum of SiO₂/Si structure with film thickness of 83 nm obtained via in situ IS measurements. (a) total spectrum and (b) focused view in low-impedance region.

Figure 6: (Color online) Impedance spectra obtained via in situ IS measurements before (0 s) and after (10–50 s) high-energy Ar⁺ irradiation. (a) total spectra and (b) focused view in low-impedance region.

Figure 7: Resistance and capacitance of SiO₂ film (R_{ox} and C_{ox}) and SiO₂/Si interface (R_{int} and C_{int}) derived by fitting of impedance spectra plotted in Fig. 6.

1 Figure 8: Resistivity ρ_{ox} (a) and dielectric constant ϵ_{ox} (b) values as function of high-
2 energy Ar^+ irradiation time. The values were calculated assuming a linear
3 decrease in the SiO_2 film thickness during Ar^+ irradiation.

4 Figure 9: (Color online) Impedance spectra obtained via in situ TDIS measurements
5 with thick SiO_2 sample (97 nm). (a) total spectra and (b) focused view in low-
6 impedance region.

7 Figure 10: Temporal variations in electrical properties of SiO_2 film (R_{ox} in (a), C_{ox} in (b))
8 and SiO_2/Si interface (R_{int} in (c), C_{int} in (d)) derived by fitting impedance
9 spectra obtained using in situ TDIS with thick SiO_2 sample (97 nm).

10 Figure 11: (Color online) Impedance spectra obtained via in situ TDIS measurements
11 with thin SiO_2 sample (20 nm).

12 Figure 12: Temporal variations in electrical properties of SiO_2 film (R_{ox} in (a), C_{ox} in (b))
13 and SiO_2/Si interface (R_{int} in (c), C_{int} in (d)) derived by fitting impedance
14 spectra obtained via in situ TDIS with thin SiO_2 sample (20 nm).

15 Figure 13: Measurement results for ex situ SE for thin SiO_2 sample (20 nm) before and
16 after plasma exposure.

17 Figure 14: Measurement results for $I-E$ curves for thin SiO_2 sample (20 nm) before and
18 after plasma exposure. Five-time measurement data for each condition are
19 plotted in the graph.

20 Figure 15: Schematics of trap creation during plasma exposure related to observed R_{int}
21 turnover. (a) phenomena in earlier phase (increase in R_{int}) and (b) those in
22 later phase (decrease in R_{int}).

1

2

3

4

5

6

7

8

9

10

Table I: Measurement results for optical thicknesses, resistivities, dielectric constants, and flat-band voltages before and after in situ TDIS experiment. The resistivity was measured from the slope of the I - E curve within a range from 0 to 1 MV/cm. The dielectric constant was calculated from the capacitance in accumulation and the optical thickness. The flat-band voltage is defined as where the capacitance becomes 90% of the value in accumulation.

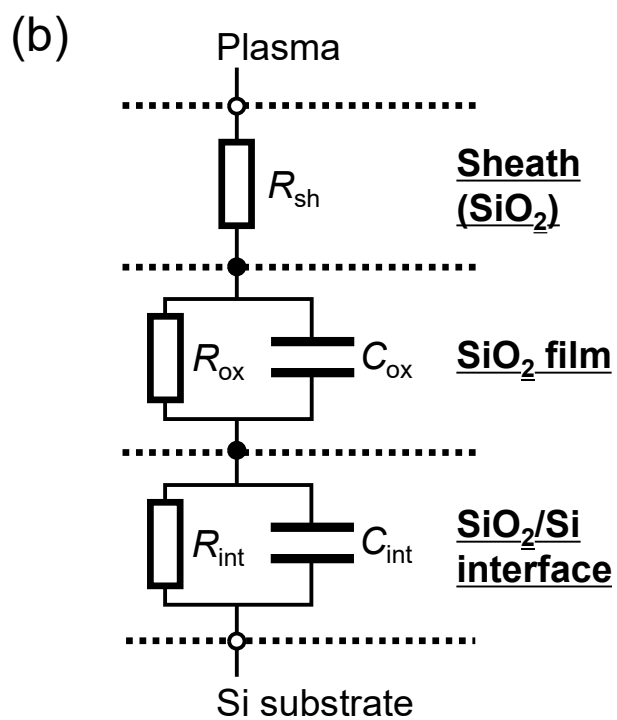
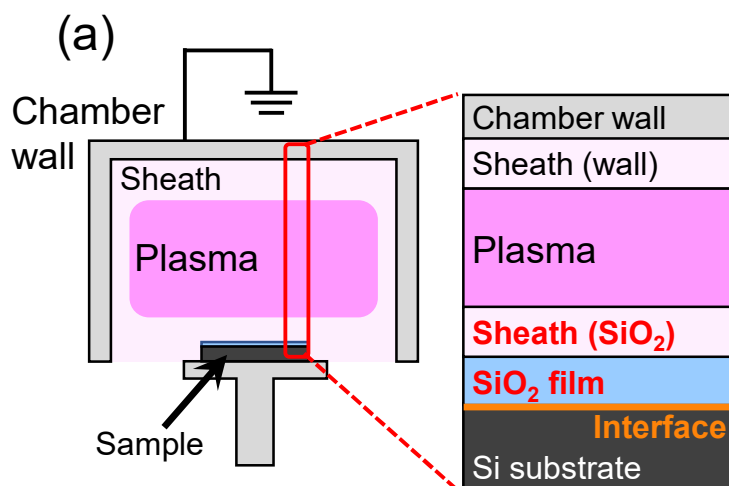
SiO ₂ /Si sample		Optical thickness	Resistivity	Dielectric constant	Flat-band voltage
Thick SiO ₂	Before	96.9 nm	$8.3 \times 10^{11} \Omega \text{ cm}$	3.8	-3.4 V
	After	96.5 nm	$9.1 \times 10^{11} \Omega \text{ cm}$	3.7	-10.9 V
Thin SiO ₂	Before	20.9 nm	$8.6 \times 10^{10} \Omega \text{ cm}$	3.7	-1.4 V
	After	20.3 nm	$3.1 \times 10^{10} \Omega \text{ cm}$	3.6	-2.2 V

11

12

1

2



3

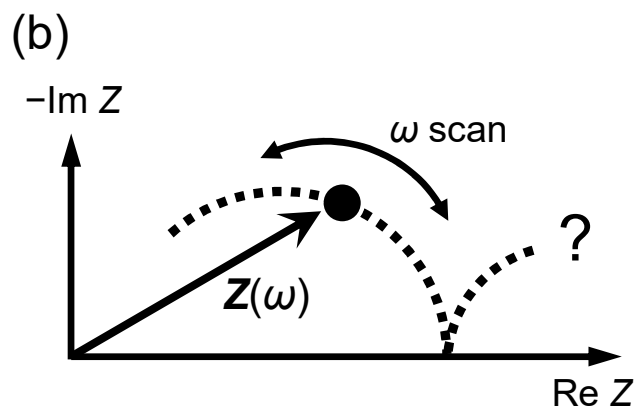
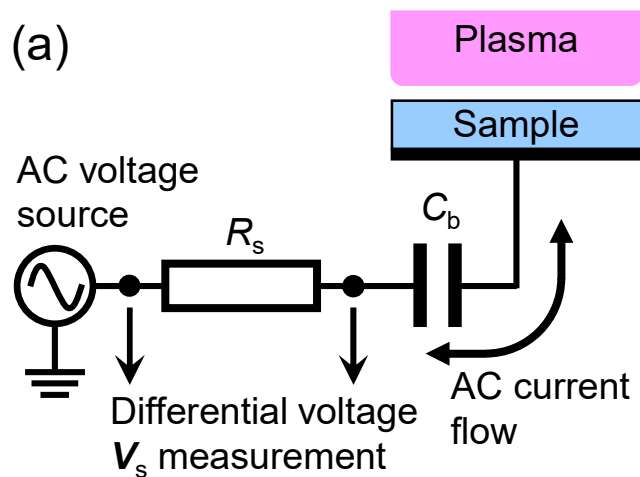
4

5

6

Figure 1

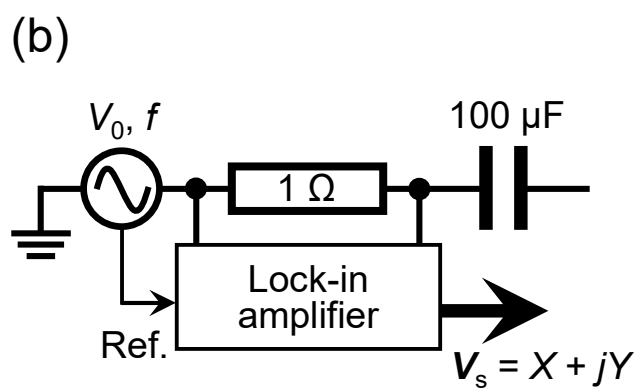
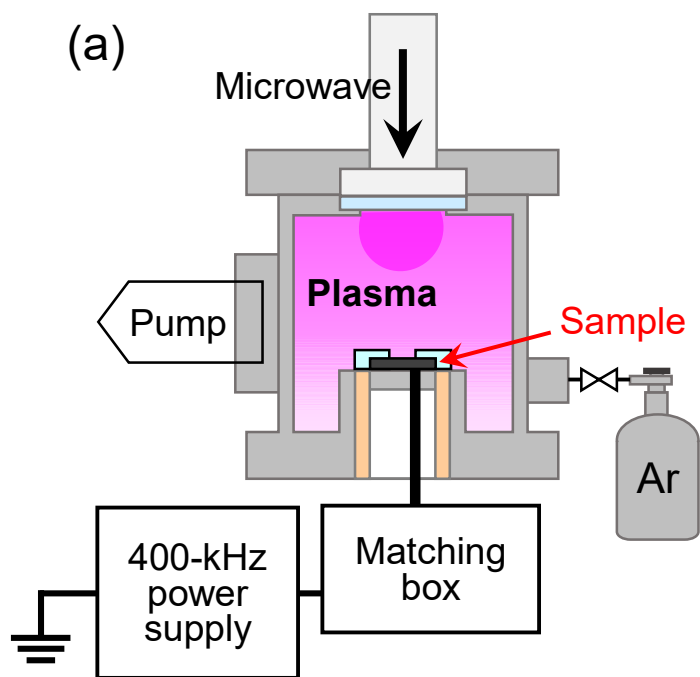
1
2
3
4
5



6
7
8
9
10

Figure 2

1
2
3
4



5
6
7
8

Figure 3

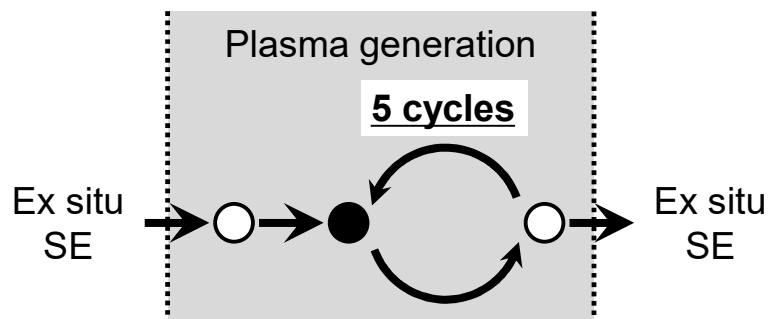
1

2

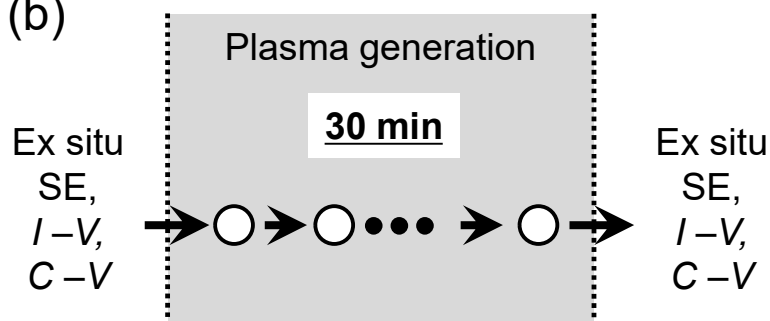
(a)

● High-energy Ar⁺ irradiation
(Plasma: ON, Bias: ON)

○ In situ IS measurement
(Plasma: ON, Bias: OFF)



(b)



3

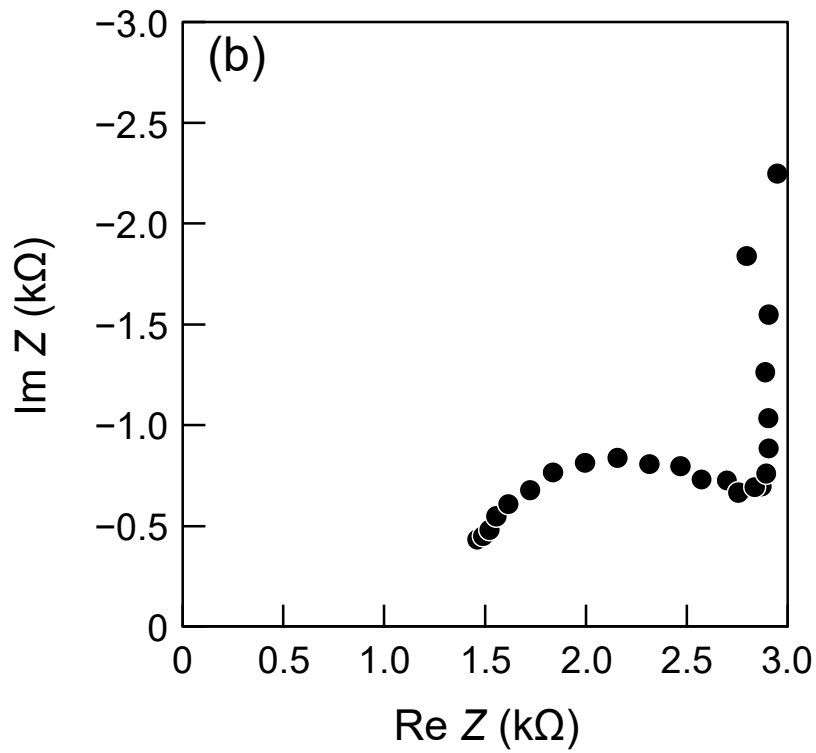
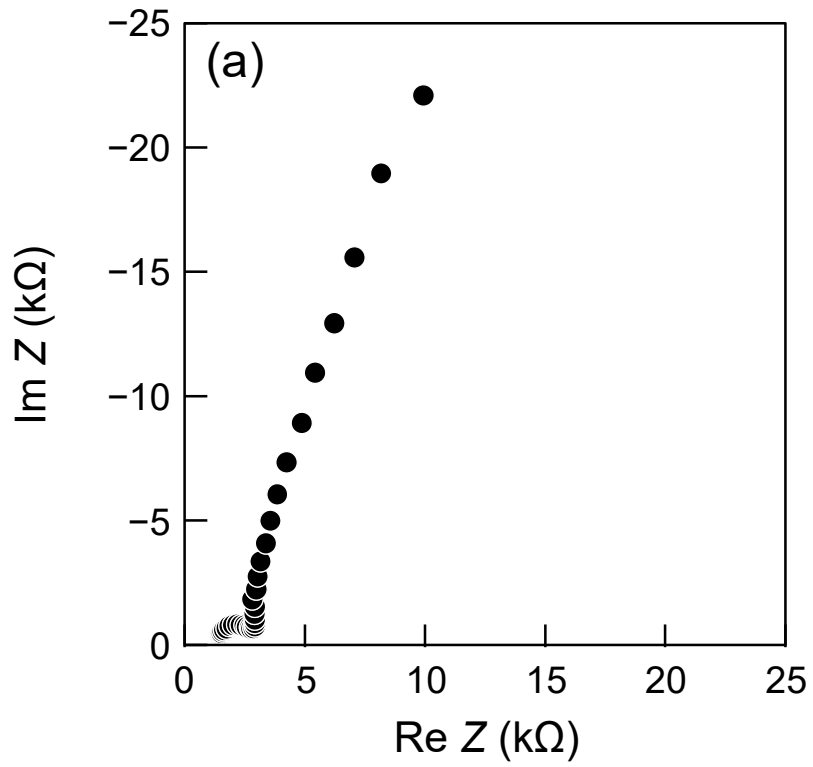
4

5

6

7

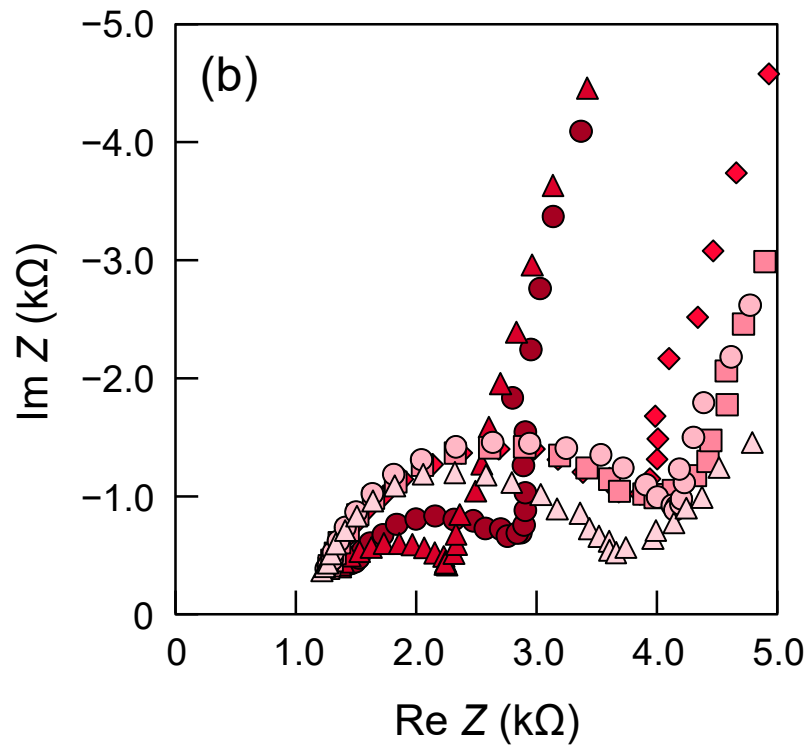
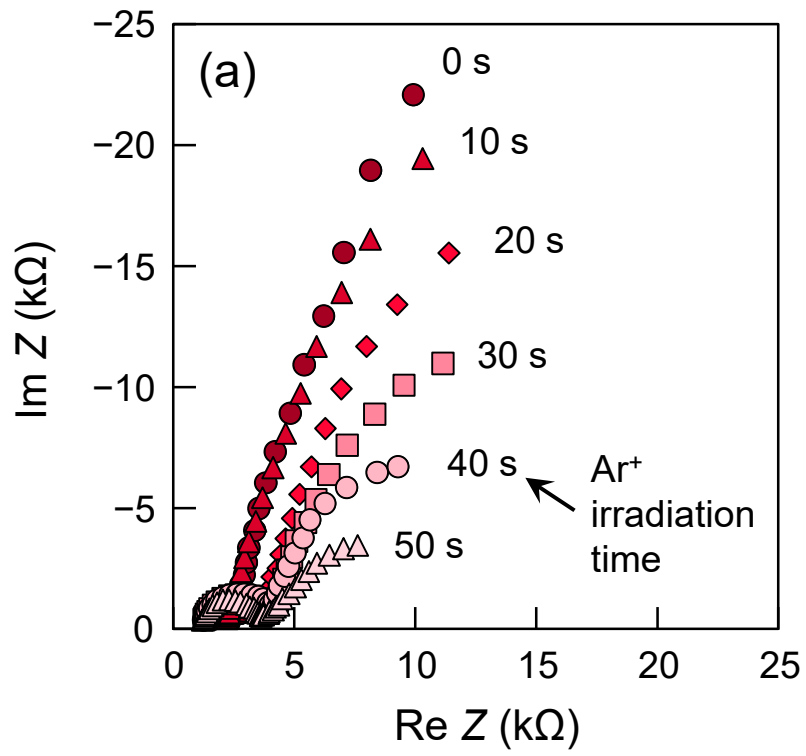
Figure 4



1

2

Figure 5



1
2
3

Figure 6

1
2
3
4
5
6
7
8
9
10
11
12
13
14
15
16
17
18
19
20
21

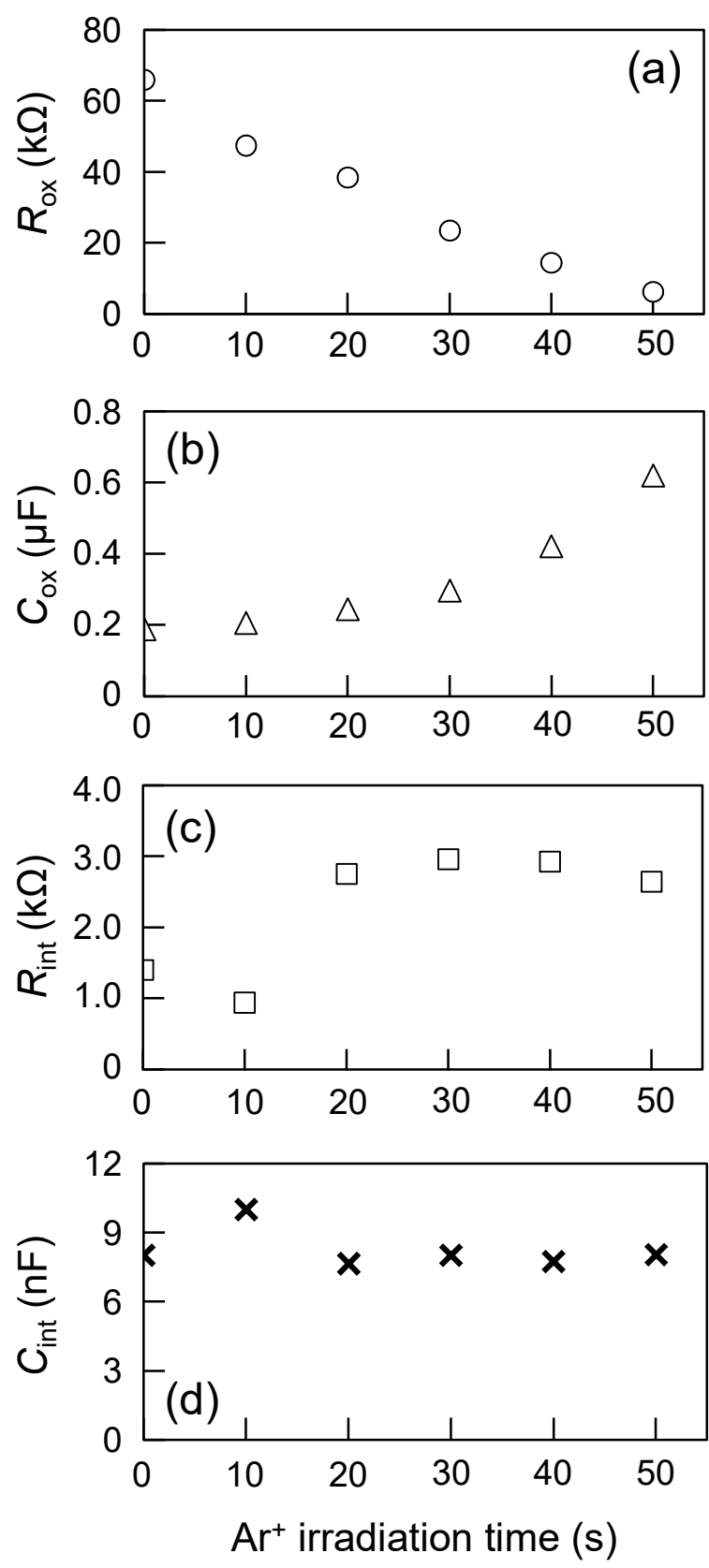


Figure 7

1
2
3
4
5
6
7
8

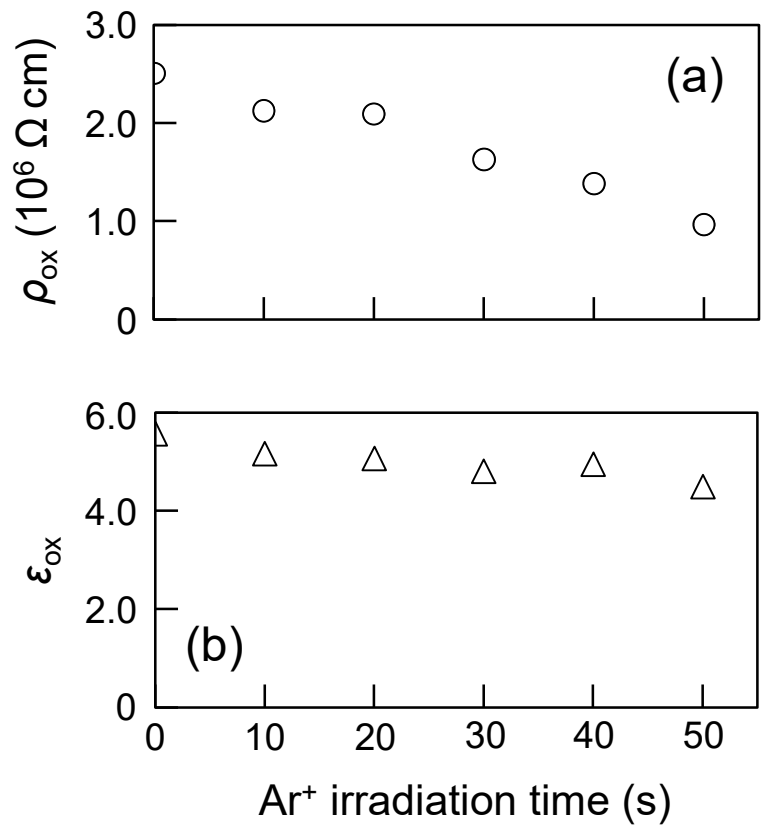
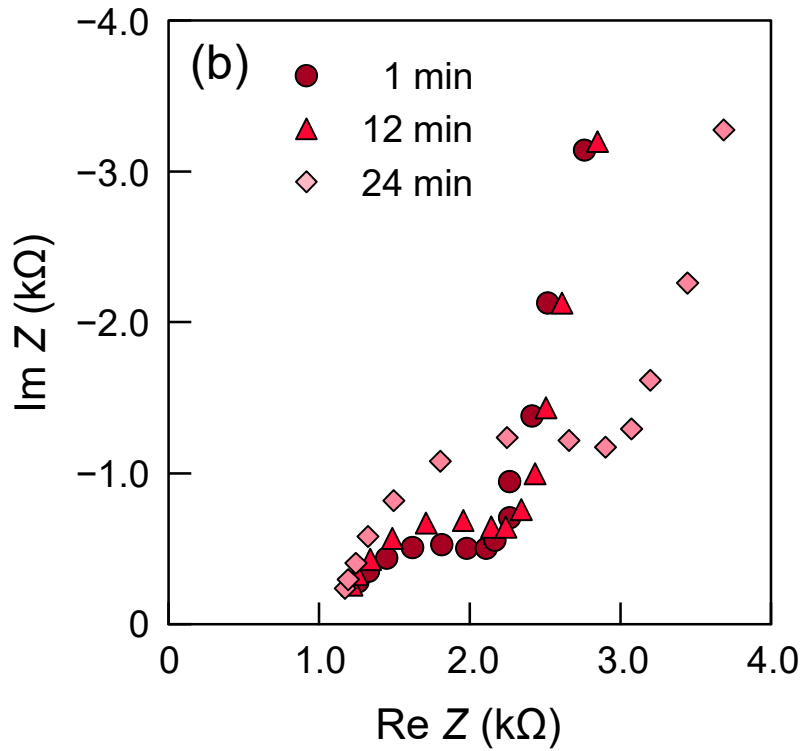
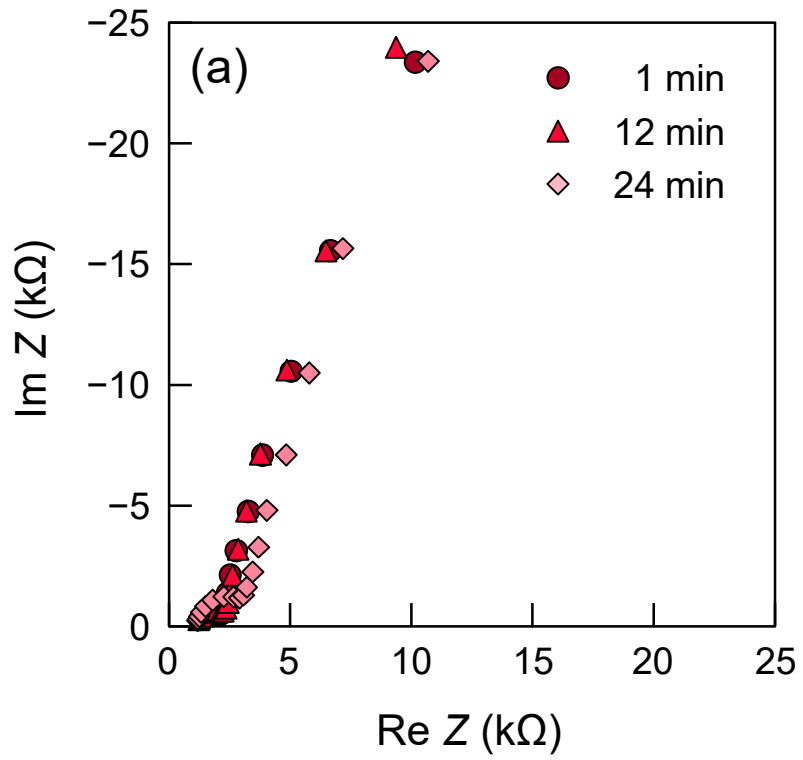


Figure 8

9
10
11
12
13
14
15



1
2
3

Figure 9

1
2
3
4
5
6
7
8
9
10
11
12
13
14
15
16
17
18
19
20
21

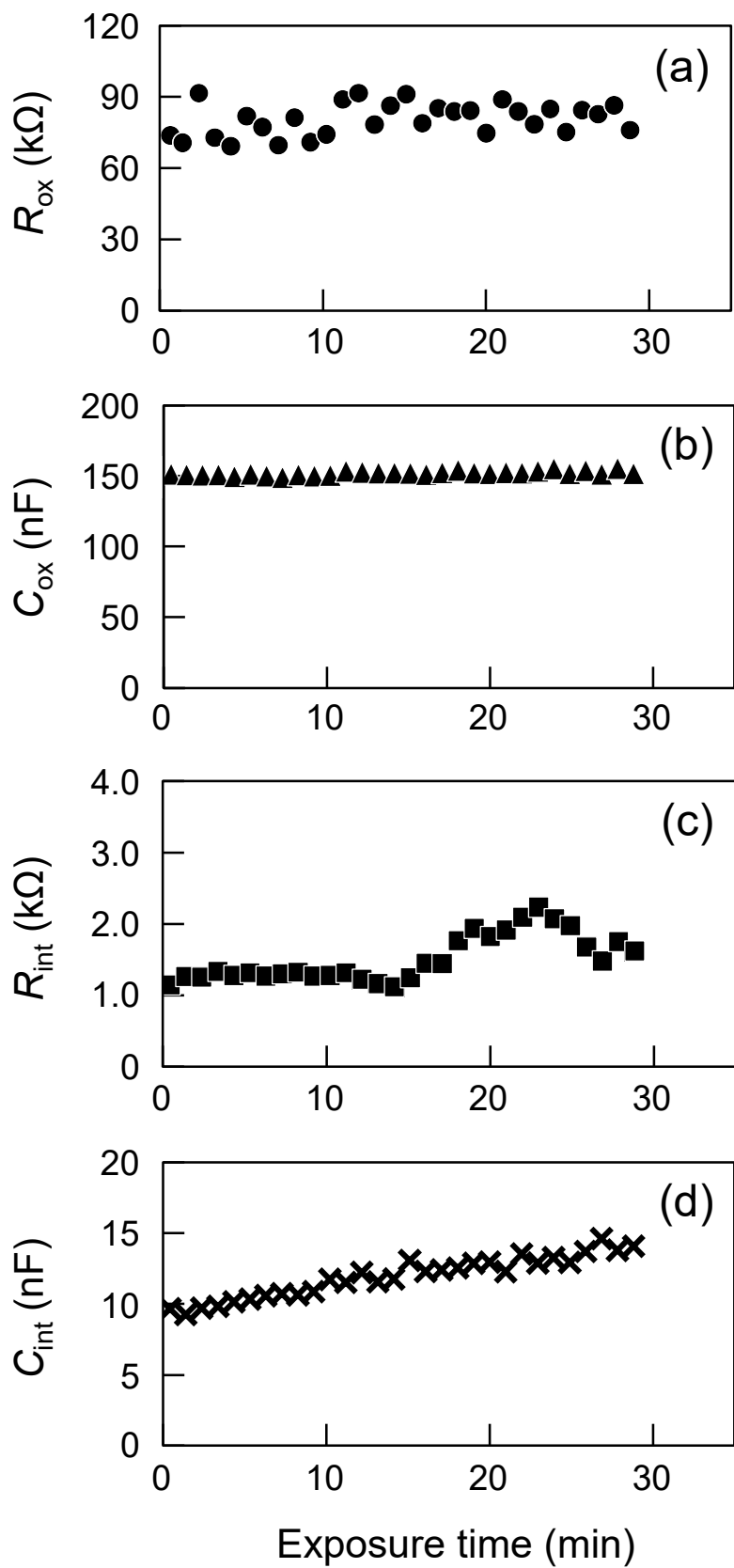
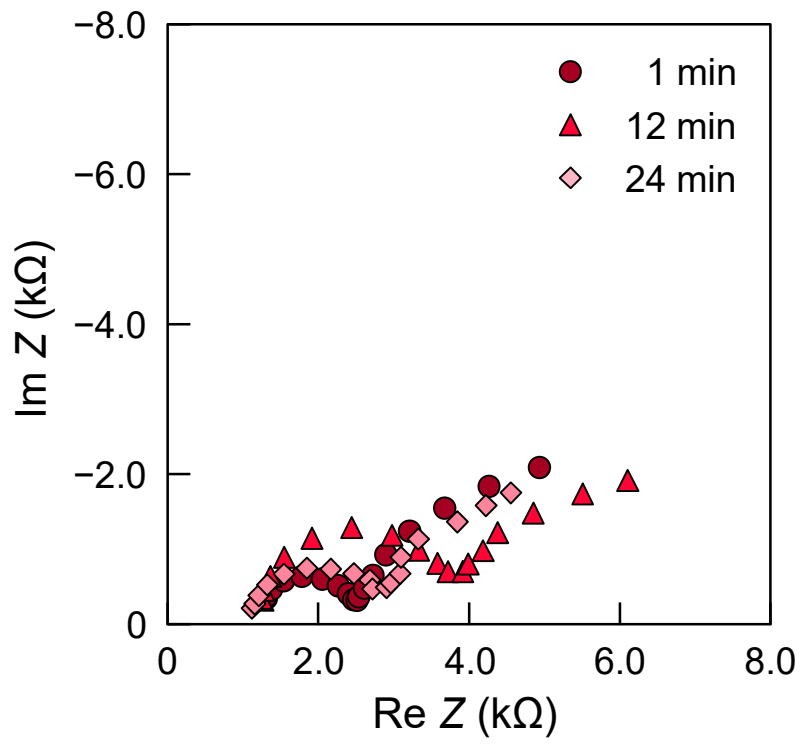


Figure 10

1
2
3
4
5



6
7
8
9

Figure 11

1
2
3
4
5
6
7
8
9
10
11
12
13
14
15
16
17
18
19
20
21

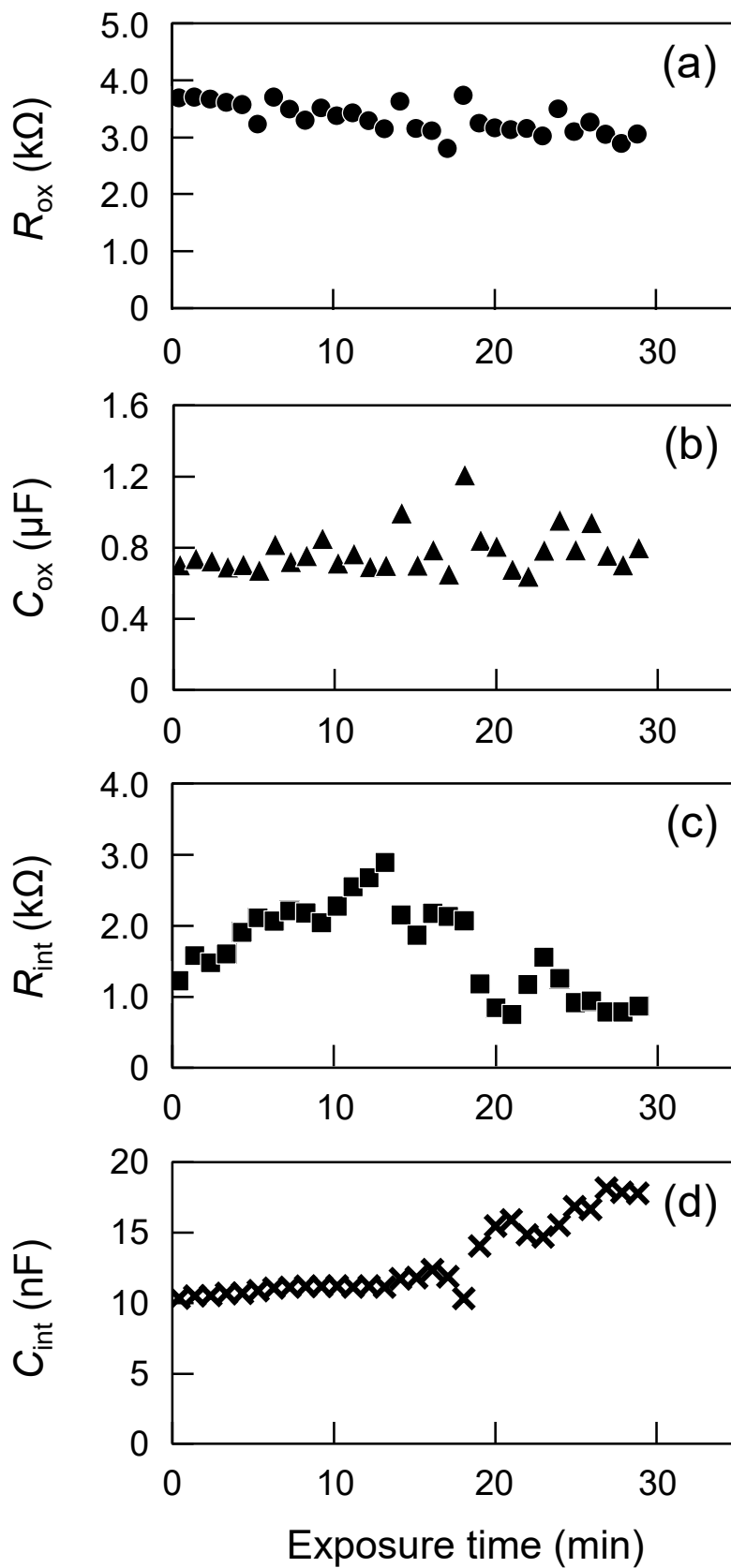
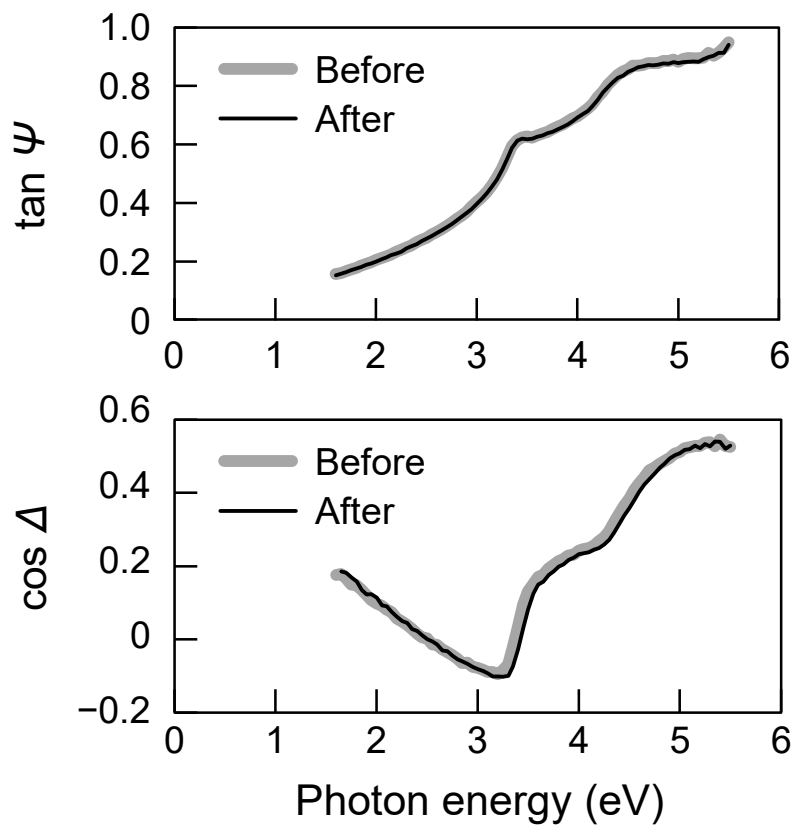


Figure 12

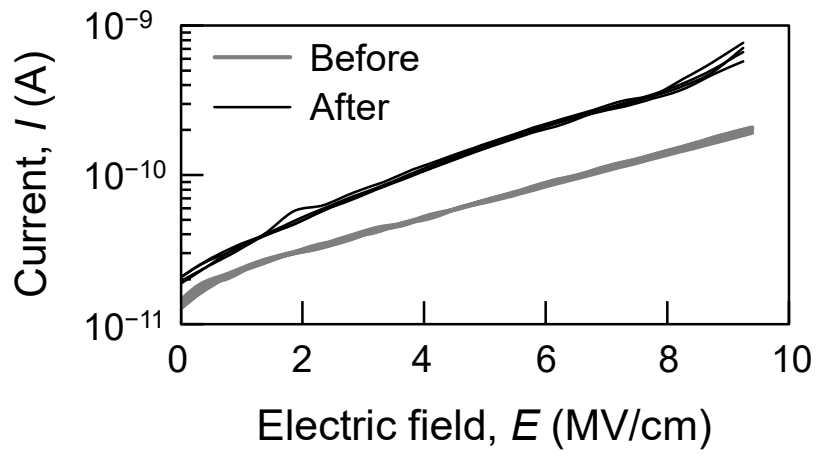
1
2
3
4
5



6
7
8
9
10

Figure 13

1
2
3
4
5
6
7

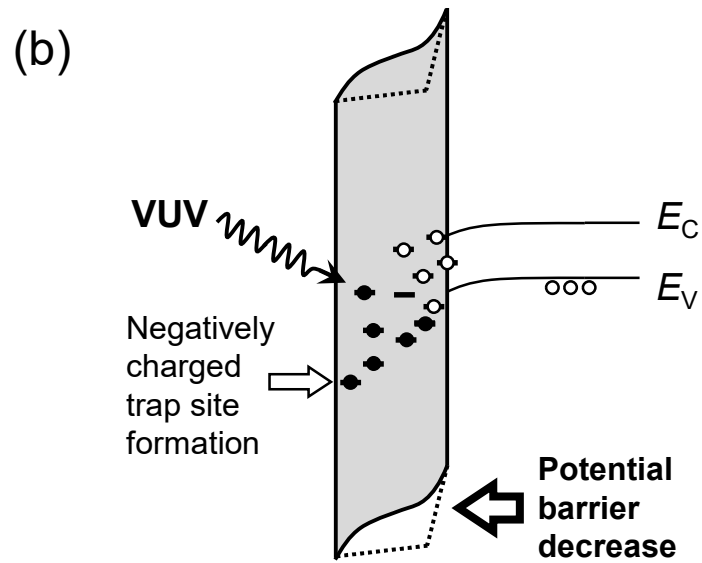
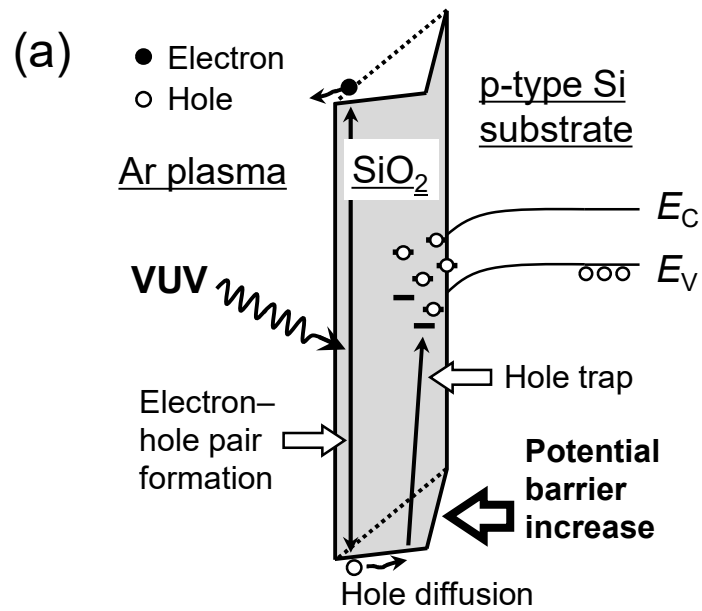


8
9
10
11

Figure 14

1

2



3

4

5

Figure 15